communications earth & environment

Article

https://doi.org/10.1038/s43247-024-01804-x

Accelerated North Atlantic surface warming reshapes the Atlantic Multidecadal Variability

Davide Zanchettin ✉ & Angelo Rubino

Observed North Atlantic sea-surface temperatures are modulated by a recurrent alternation of anomalously warm and cold interdecadal phases known as Atlantic Multidecadal Variability. Here we use observations and a multi-model ensemble of climate simulations to demonstrate an ongoing acceleration of North Atlantic surface warming, which implies a smaller contribution of the Atlantic Multidecadal Variability to 21st century North Atlantic sea-surface temperature anomalies than previously thought. Future projections of the Atlantic Multidecadal Variability from realistic climate simulations are poorly constrained, yet a relaxation to a neutral phase by the mid-21st century emerges as the most probable evolution of the Atlantic Multidecadal Variability. In the simulations, the mitigating effects of a less likely upcoming cold phase of the Atlantic Multidecadal Variability are overwhelmed by fast North Atlantic surface warming, which is robustly projected to persist in upcoming decades independent of emission scenarios. Sustained North Atlantic surface warming is therefore expected to continue in the near future.

Earth's surface temperatures were exceptionally high in 2023, which resulted in the warmest calendar year on record[1]. The 2023 global anomaly is shaped by exceptional regional anomalies, including a record minimum extent of Antarctic sea ice[2], the ongoing 2023/24 El Niño in the equatorial Pacific, and surface warmth of the North Atlantic Ocean[3,4] Attribution of the 2023 global climate anomaly thus requires understanding the relative role of external forcings, primarily the increased atmospheric greenhouse gas concentrations (IPCC-AR6), possibly temporarily enhanced by the submarine Hunga-Tonga volcanic eruption in 2022[5], and intrinsic dynamics and phenomena contributing to regional climate variability[6]. Therefore, the 2023 global climate anomaly and the recent sequence of exceptionally warm years before 2023 call to reconsider some paradigms invoked for the description and interpretation of regional climatic phenomena, especially as far as the separation between centennial trends and higher-frequency variability is concerned. Here, we use observations and simulations to demonstrate that the Atlantic Multidecadal Variability (AMV) is less important than currently thought for explaining recent historical and future projected climate anomalies and trends.

The classic view of the AMV consists of a recurrent alternation of interdecadal phases of surface warming and cooling of the North Atlantic Ocean[7]. In historical times this was observed as an apparent 60-year oscillation in basin-average North Atlantic sea-surface temperatures (SSTs) superposed on a secular warming trend, with two interdecadal cold phases centered approximately around 1900–1925 and 1965–1995, and three interdecadal warm phases centered approximately around 1870–1900, 1930–1960 and 1995–present (Fig. 1a, b, see also ref. 8). The observed spatial pattern of the AMV presents a pan-basin signature over the North Atlantic, with large positive regression coefficients in a comma-shaped pattern centered in the western subpolar gyre region and extending south-eastward along the eastern boundary and further spreading westwards along the tropical band, with weaker signals in the western subtropical gyre region (Fig. 2a). This pattern reflects the diversity of processes contributing to the AMV[9]. Whether the historical AMV is predominantly externally forced or intrinsically induced remains debated, especially regarding the role of tropospheric aerosols, at least for the most recent cold AMV period[10–14]. The presence, in the North Atlantic, of coupled dynamics linked to the active thermohaline circulation has important implications for the AMV and its predictability[8,15]. Near-term scenarios of future AMV evolution that build on observations point to the possibility of an incipient cold phase of the AMV after the current warm phase established in the 1990s[16,17] However, despite the North Atlantic being considered to feature strong potential decadal climate predictability, the predictable signal is hidden by a low signal-to-noise ratio in current climate models[18] and model-based evidence for an imminent cooling of the upper North Atlantic remains limited to the subpolar gyre region[19,20].

Below, we demonstrate how an ongoing acceleration of North Atlantic surface warming implies that the current warm AMV phase has a smaller

University Ca' Foscari of Venice, Department of Environmental Sciences, Informatics and Statistics, Via Torino 155, 30172 Mestre, Italy.
✉e-mail: davidoff@unive.it

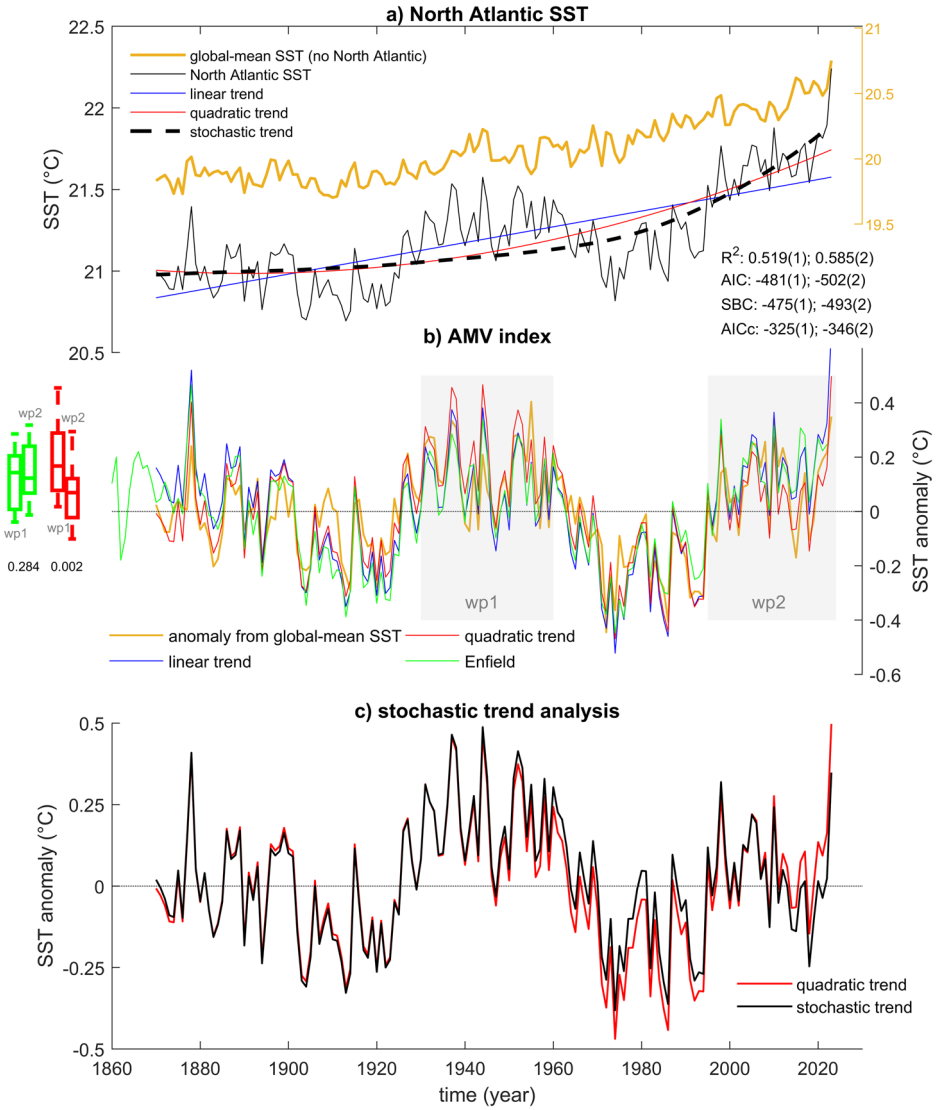

Fig. 1 | Historical North Atlantic SST and AMV index. a Observed annual time series of average global and North Atlantic SST (HadISST) and three trend estimates for the latter (1870–2023) with associated metrics including coefficient of determination (R^2), Akaike's information criterion (AIC), Schwarz's Bayesian criterion (SBC) and corrected AIC (AICc) for the linear (1) and quadratic (2) models. **b** Observed AMV indices obtained from detrending North Atlantic SST using a linear and a quadratic regression model, and as deviation of North Atlantic from global-mean SST excluding the AMV domain (1870–2023), and their comparison with the Kaplan SST AMO index by ref. 7; the boxplot illustrates the distributions (median, 25–75 percentile range, extremes) of the Kaplan SST AMO index (green) and for the quadratic detrended AMV index (red) for the warm phases of 1930–1960 (wp1) and 1995–2023 (wp2); below the boxplots are *p*-values for a rank sum test comparing wp1 and wp2 data; **c** Observed AMV index obtained as residual from the stochastic trend of North Atlantic SST.

amplitude than previously thought, revealing a strongly damped nature of the AMV. Accordingly, we show that simulations from a multi-model ensemble of *historical* and global warming scenario (*ssp585* and *ssp245*) simulations contributing to the sixth phase of the coupled model intercomparison project (CMIP6[21,22] and realistically representing the historical AMV yield an expected neutral phase before the mid-21st-century. A total of 176 simulations from 29 models are considered, most of which provide more than one realization: up to 25 realizations for CanESM5, 29 realizations for MPI-ESM1-2-LR, and 40 realizations for ACCESS-ESM1-5.

Results

A crucial aspect of the analysis is a consistent separation, in observations and simulations, of the multi-decadal AMV signal from the long-term global warming signal. Different methods exist to calculate the AMV index[9,23] that capture different aspects of the considerable regional structure of North Atlantic SST anomalies and their connection with the global-mean SST (Fig. 1a). As of today, nonetheless, a basin average with linear detrending of North Atlantic average SST remains typically adopted[7,24] We assert that the assumption of a constant trend during the observational period is not well posed based on the following arguments that point to an acceleration of North Atlantic surface warming.

First, comparing regression models of observed North Atlantic SST on time (1870–2023) yields a quadratic fit to perform better than a linear fit according to several metrics, including coefficient of determination (R^2), Akaike information criterion (AIC) and Schwarz's Bayesian criterion (SBC) (Fig. 1a). Similar results are obtained excluding from the analysis the most recent years, which indicates that this acceleration does not merely result from a short sequence of exceptionally warm years (e.g., for the period 1870-2018, quadratic trend: $R^2 = 0.518$; AIC = −490; SBC = −481; linear trend: $R^2 = 0.474$; AIC = −480; SBC = −474). Furthermore, a quadratic fit outperforms a linear fit to describe local SST trends over most parts of the North Atlantic, including key AMV regions such as the western subpolar gyre and the eastern tropics (Fig. 2a). An observational AMV index obtained as a residual from a quadratic fit to basin-average North Atlantic SST yields 21st-century AMV warm anomalies that have significantly smaller amplitudes compared to mid-20th-century AMV warm anomalies, in contrast to the classical AMV index where both warm anomalies have comparable amplitude (boxplots in Fig. 1b). This succession of warm phases with decreasing amplitudes describes the historical AMV evolution as characterized by damped, in contrast to regular, fluctuations.

Trends of observed global-mean SST supports the hypothesis that acceleration of North Atlantic surface warming is part of a global phenomenon (for the period 1870–2023, quadratic trend: $R^2 = 0.965$; AIC = −750; SBC = −741; linear trend: $R^2 = 0.778$; AIC = −676; SBC = −670). Accordingly, an AMV index calculated as deviation of North Atlantic SST from the global-mean SST excluding the AMV domain yields a mid-20th-century AMV anomaly (0.135 °C for the period 1930–1960) that is slightly warmer than 21st-century AMV anomaly (0.095 °C for the period

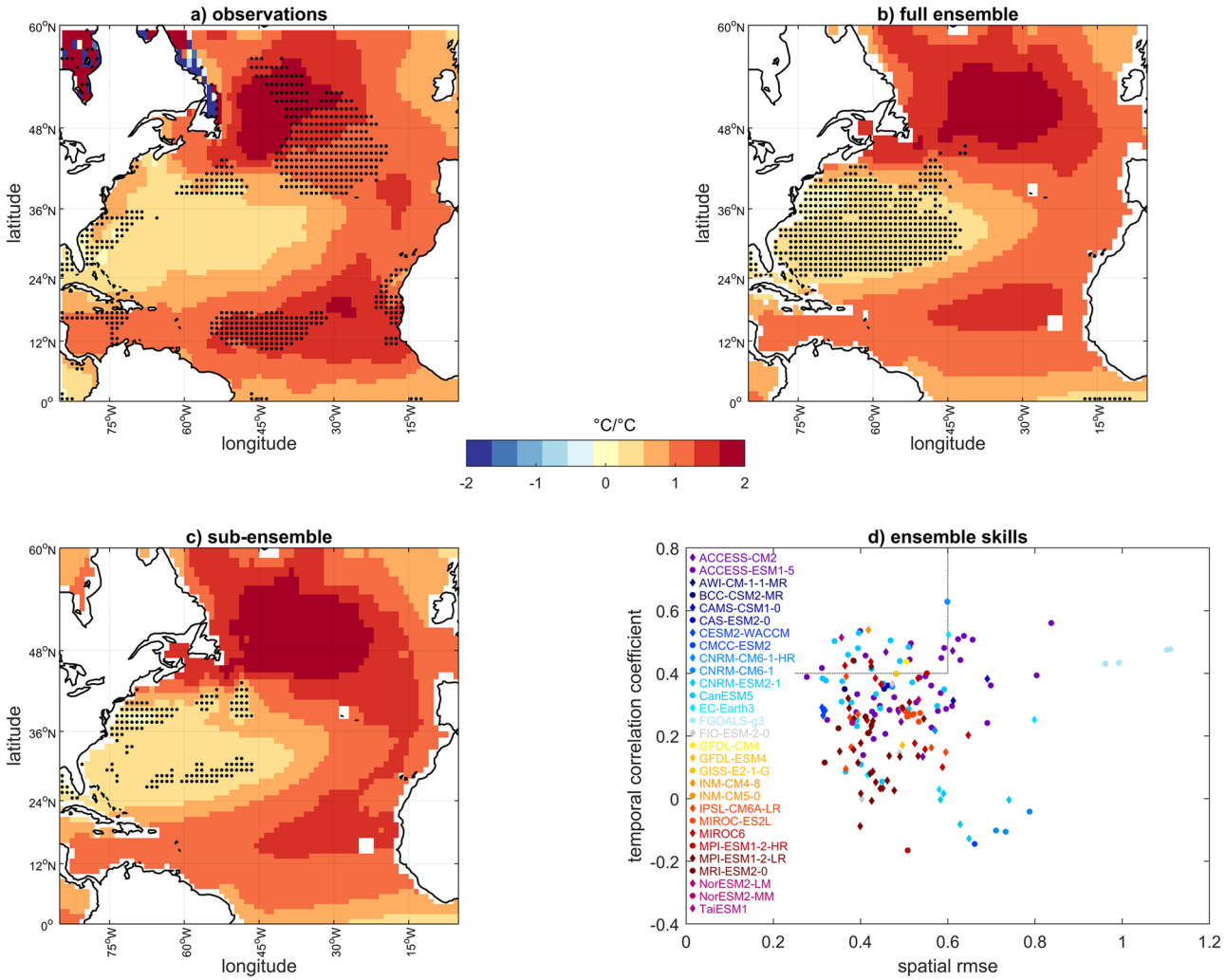

Fig. 2 | Historical spatial pattern of the AMV in observations and simulations. **a**–**c** Regression of the AMV index (dlm) on North Atlantic SST (period 1900–2023, quadratic trend removal) for **a** observations (HadISST), **b** the full multi-model ensemble of CMIP6 historical simulations, and **c** the sub-ensemble with simulations most realistically representing the observed AMV (AMV sub-ensemble); **d** evaluation of the CMIP6 ensemble in terms of spatial and temporal representation of the observed AMV. Dots in panel **a** indicate where a linear fit is statistically preferable than a quadratic fit to explain the local SST trend; dots in panels **b**, **c** indicate where there is disagreement across models in the sign of the AMV signature on local SST (at least 10% of the models disagree on the sign). In panel **d**, the upper-left region encompassed by the dotted black lines identifies the candidate simulations contributing to the AMV sub-ensemble.

1995–2023), both warm periods being not significantly different ($p = 0.26$). The damped nature of the AMV is therefore rejected if assuming that the AMV has no active role in surface warming of the global ocean—a hypothesis that, however, contrasts with model-based evidence that the AMV is a source of decadal global SST variability[25–27].

To separate the AMV signals from the accelerated warming of the North Atlantic average SST we use a dynamic linear model (dlm) framework[28] where long-term warming is assumed to evolve according to a weakly varying stochastic trend (see methods). Steepening of the stochastic trend slope around 1970 pinpoints the start in the acceleration of North Atlantic surface warming (Figs. 1a and 3b). The observational AMV index calculated as the residual after removal of the stochastic trend from the basin-average North Atlantic SST data (Fig. 1c) is practically indistinguishable from the AMV index obtained assuming a quadratic trend ($r = 0.97$, $p \sim 0$) and shows even cooler 21st-century conditions.

Multiple observational lines of evidence thus indicate that the observed 21st-century North Atlantic surface warming include a smaller contribution from positive AMV anomalies than currently considered. If North Atlantic surface warming has accelerated, then the AMV has a damped nature.

Climate models provide additional evidence of an ongoing acceleration of North Atlantic surface warming, supporting that the current warm phase of the AMV is weaker than previously thought. Our multi-model ensemble of CMIP6 *historical+ssp585* simulations shows that different models yield largely different 21st-century North Atlantic surface warming (Fig. 3a), ranging from reaching +1.2 °C in GISS-E2-1-G to +6 °C in CanESM5 by 2100 with respect to the 1870–2023 average, which possibly reflects the different climate sensitivities across the multi-model ensemble[29]. Despite this model diversity, the agreement across models in a steepening of trajectories in recent decades is apparent. To quantify this acceleration, like what is done for observations, we use a dynamic linear model to extract the expected long-term warming signal from the raw basin-average North Atlantic SST data, assuming the long-term warming evolves according to a weakly varying stochastic trend. Despite the large model uncertainty, in strong agreement with observations, stochastic trends are consistently larger in the most recent decades, starting from the 1970s, than in the preceding period (Fig. 3b). Therefore, despite the large uncertainty in projected 21st-century North Atlantic warming, models consistently describe an ongoing acceleration of North Atlantic surface warming.

The stochastic trend removal allows for a seamless AMV signal throughout the period 1850-2099 in each simulation of the CMIP6 multi-model ensemble (Fig. 3c). The contributing models generally capture the gross features of the observed temporal development of the AMV: In the full

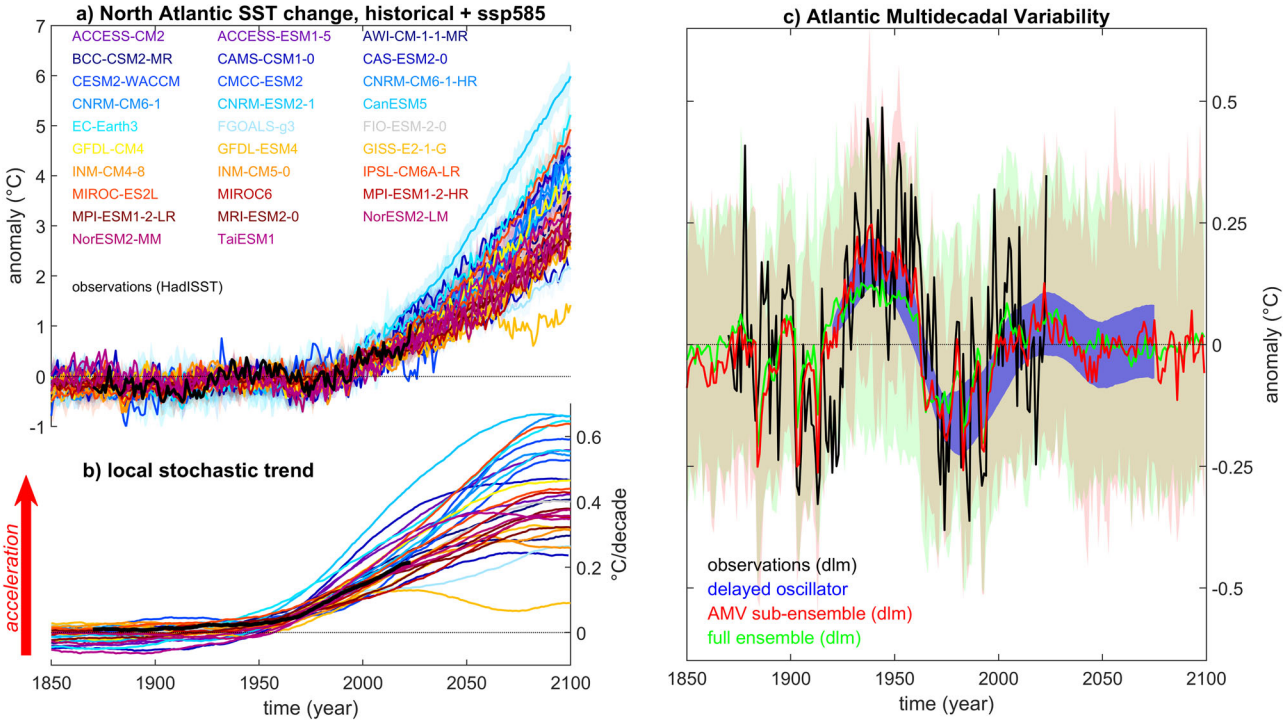

Fig. 3 | Simulated historical and projected (ssp585) North Atlantic SST and AMV index. a, **b** Evolution of annual spatially averaged North Atlantic SST for single-model ensembles (line: mean; shading: 5–95 percentile range) (**a**) and associated local stochastic trend (**b**) with comparison with observations (HadISST, black line); **c** evolution of simulated AMV with stochastic trend removal from the dynamic linear model (dlm) and for different ensembles (full ensemble and sub-ensemble with simulations that best represent the observed AMV; line: mean; shading: 5–95 percentile range). The blue shading illustrates the evolution (5–95 percentile range) for an ensemble of delayed AMV oscillators with a range of delay times from interannual to interdecadal.

ensemble, the simulated AMV in the historical period compares well with the observed AMV index (dlm), with the ensemble mean featuring an alternation of warm and cold interdecadal anomalies with similar amplitude and in rough co-phase with the observed anomalies (green line in Fig. 3c). This emerging coherent phasing suggests that the historical AMV is strongly imprinted by external forcing: volcanic eruptions in the late 19th century and increased anthropogenic tropospheric aerosol in the second half of the 20th-century[8]. Nonetheless, temporal coefficient of correlation (r) and temporal root mean squared error (rmse) reveal a large diversity of skills in representing AMV characteristics across models (e.g., $r_{\text{CNRM-CM6-1-r2}} = 0.610$; $r_{\text{CMCC-ESM2-r1}} = -0.130$; $\text{rmse}_{\text{INM-CM4-8-r1}} = 0.016$; $\text{rmse}_{\text{EC-Earth3-r1}} = 0.036$) and realizations from the same model (e.g., $r_{\text{ACCESS-SM1-5-r25}} = 0.563$; $r_{\text{ACCESS-SM1-5-r3}} = 0.137$; $\text{rmse}_{\text{MPI-ESM1-2-HR-r1}} = 0.019$; $\text{rmse}_{\text{MPI-ESM1-2-HR-r2}} = 0.027$). Similar considerations stand for the spatial pattern of the AMV as seen in the largely coherent comma-shaped ensemble-mean signature on North Atlantic SSTs (Fig. 2b). Metrics such as spatial correlation and spatial rmse reveal, nonetheless, substantial diversity across models and across realizations from the same model in representing the observed AMV spatial patterns (e.g., spatial $r_{\text{ACCESS-ESM1-5-r13}} = -0.202$; spatial $r_{\text{ACCESS-ESM1-5-r19}} = 0.363$; spatial $\text{rmse}_{\text{CNRM-CM6-1-r6}} = 0.350$; spatial $\text{rmse}_{\text{MIROC6-r2}} = 1.253$). Overall, despite the good general performance of some models (most noticeably ACCESS-ESM1-5 and CanESM5), the scattered skills for all single-model ensembles (Fig. 2d) prevent identifying key model specificities that contribute to the realism of the simulated AMV and rather point to a substantial contribution by intrinsic variability.

The sub-ensemble with the best-performing realizations (AMV sub-ensemble, see methods) maintains a realistic spatial pattern of the AMV, more robust across models than the full ensemble (Fig. 2c), while yielding substantial improvement in the spread of temporal AMV evolution compared to the full ensemble, indicative of stronger coherent phasing across simulations especially since the 1930s (red line in Fig. 3c). Again, this sub-ensemble yields 21st-century warm anomalies of the AMV with smaller amplitudes compared to mid-20th-century warm anomalies and with spread largely encompassing also negative values. The high skills and coherency of simulations within the AMV sub-ensemble are not tied to their representation of ocean dynamics: Whereas models within the AMV sub-ensemble provide a strongly consistent spatial structure of the Atlantic meridional overturning circulation (AMOC) (Fig. 4a), the AMV imprint on the AMOC is largely incoherent across models, except for the shallow mid-altitude and polar North Atlantic (Fig. 4b). The large spread of cross-correlation profiles between AMV and two AMOC indices for individual simulations within the AMV sub-ensemble confirms the diversity of behavior across models and across realizations with the same model (Fig. 4c, d). For instance, a near co-phase between AMV and AMOC is consistently found in two realizations from different versions of the MPI-ESM model, or in most realizations with CanESM2, whereas it is impossible to discern a preferred phase-relation within ACCESS-ESM1-5 or CNRM-CM6-1 in terms of sign, strength or timing. This diversity of coupling between AMV and ocean circulation stems from several potential causes, including model specificities regarding the time scale and amplitude of intrinsic AMOC variability[30] and the disruption of intrinsic AMV-AMOC dynamics by external forcing[8]. Therefore, assuming the role of ocean circulation for the AMV, no dominant mechanism emerges to explain the ensemble historical AMV evolution.

In the scenario period, the simulations quickly lose coherence even in the AMV sub-ensemble, contrasting with their tight constraints on the 20th-century evolution. Large spread and small amplitude of multi-decadal fluctuations in the mean of the AMV sub-ensemble suggest weak consistency across models and realizations. Still, emerging tendencies include the current weak warm phase lasting till the late 2030s and the following neutral phase persisting through the 2050–60s. Empirical trend estimates (Fig. 5d) confirm the expected onset of an interdecadal period with weak, yet significant, AMV cooling in the early 2040s, which mitigates but does not overwhelm the long-term North Atlantic warming under the strong

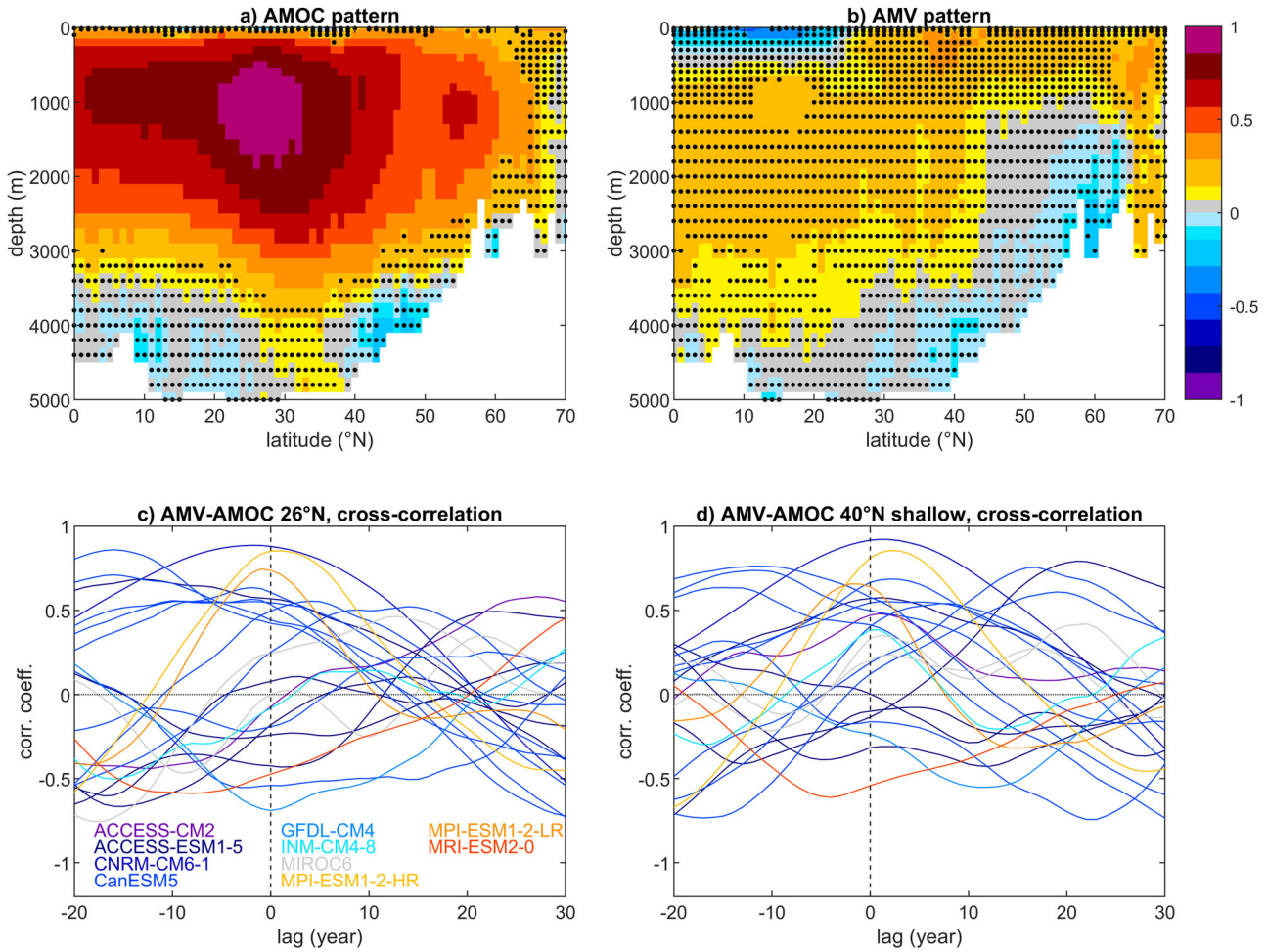

Fig. 4 | Relation between simulated AMV and ocean circulation in the AMV sub-ensemble. **a**, **b** Ensemble-mean lag-0 correlation pattern (period 1870-2014) of the Atlantic meridional overturning streamfunction describing the AMOC with **a** the AMOC index at 26°N, 1000 m depth, and **b** the AMV index (stochastic trend removal); **c**, **d** cross-correlation between the AMV index and **c** the AMOC index at 26°N, 1000 m depth and **d** the AMOC index at 40°N, 300 m depth, for individual simulations. In panels **a**, **b** dots indicate where at least 25% of the models in the AMV sub-ensemble disagree on the sign of the correlation. The AMV leads to negative lags. AMOC data detrended with a 2nd-order polynomial fit, and all data smoothed with a low-pass filter (11-year running average). GISS-E2-1-G r1 data is not available.

emission scenario considered here (Fig. 5c). This is in clear contrast with the simulated historical behavior where AMV trends dominated North Atlantic SST trends up to the interdecadal time scale. This, again, points to a strongly damped nature of the phenomenon. Accordingly, the simulated AMV is consistent with a range of damped oscillators with time delays from inter-annual to interdecadal (blue shading in Fig. 3c, see methods), suggesting that the AMV is part of a self-excited damped mode of climate variability.

The *ssp585* scenario provides for a sustained warming signal throughout the 21st-century but is considered implausible by recent assessments[31,32]. The milder *ssp245* scenario provides for more realistic projected climates, but it also makes the long-term trend and AMV components of 21st-century evolution of North Atlantic SST less discernible, as the warming trend weakens before the mid of the century following the applied forcing pathway (Fig. 5a, e). The multi-decadal time scale of this forced evolution superposes on the typical AMV time scale, complicating the separation between variability arising from North Atlantic dynamics and transient response to radiative forcing. In the scenario period, forced trends from the AMV sub-ensemble still indicate sustained North Atlantic surface warming in the next couple of decades for *ssp245*, like what is obtained for *ssp585* (Fig. 5e). Larger trends are also consistently pictured by both scenarios since the 1970s: an ongoing acceleration of North Atlantic warming is therefore a robust feature across simulations, models and scenarios.

In the historical period, the dynamic linear model yields a slightly stronger warming trend around the mid-20th-century, followed by a stronger cold AMV phase in the *ssp245* compared to the *ssp585* scenario (Fig. 5a, b). Therefore, a statistical separation between direct radiative response to forcing, dynamical responses, and intrinsic variability cannot be clear-cut. The amplitude of this uncertainty is comparable to that found for different trend models accounting for accelerated warming in observations (Fig. 1c). Despite these uncertainties, the AMV sub-ensembles from both scenarios agree on the stark contrast between large and coherent historical AMV fluctuations, and large spread in projected AMV evolution yielding vanishing expected anomalies in the scenario period (Fig. 5b, d, f).

Discussion

The proposed characterization of the historical AMV with a damped early 21st-century warm anomaly has extensive implications for the detection and attribution of recent changes in regional climates impacted by the AMV[7,33], the reconstruction of the AMV[34], and its attribution[10–12,35] and dynamical interpretation[8,17,36]. Still, constraining the near-future evolution of the AMV and North Atlantic surface temperatures remains a challenge. The found diversity of AMV-AMOC connections within the AMV sub-ensemble reveals a variety of expressions of simulated dynamics that necessarily have different levels of realism. Furthermore, only in individual realizations the intrinsic component of the AMV is fully expressed. Based on individual simulations and accounting for scenario uncertainty—that is, merging the *ssp585* and *ssp245* AMV sub-ensembles—a neutral AMV phase (2040–2060 average within ±0.1 °C) by the mid-21st-century is the most

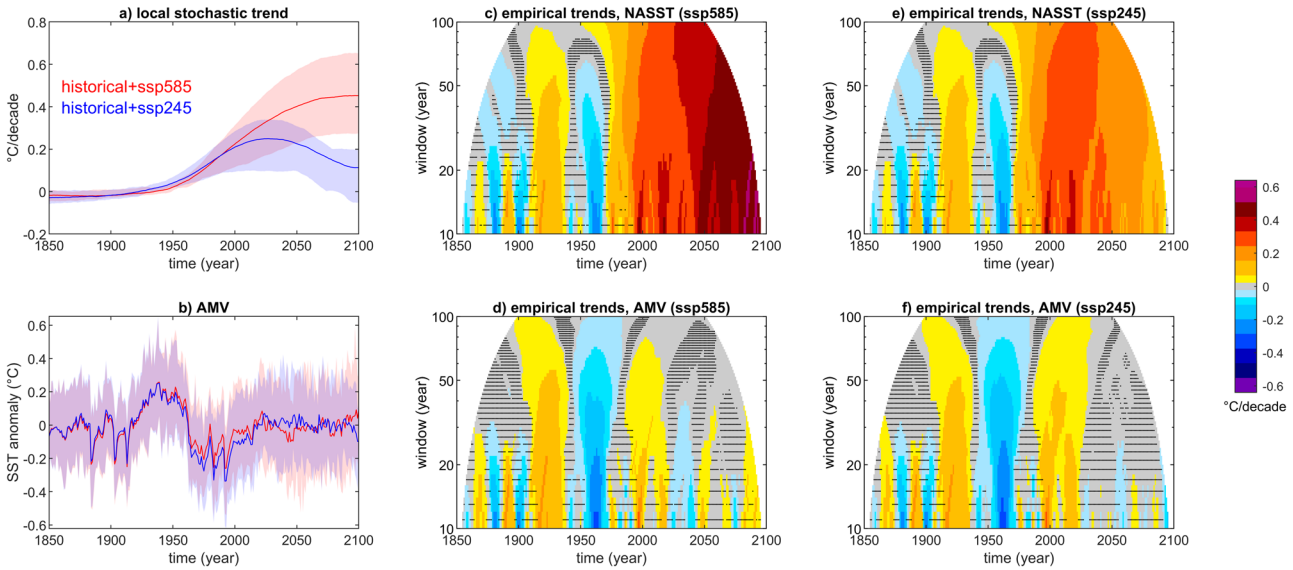

Fig. 5 | The role of different warming scenarios. a, **b** ensemble average (line) and spread (5–95 percentile range, shading) of the local stochastic trend (**a**) and AMV index (**b**) for the *ssp585* and *ssp245* scenarios in the AMV sub-ensemble; **c**, **e** time-length diagram of empirical linear trends of the AMV sub-ensemble average of spatially averaged North Atlantic SST for the *ssp585* (**c**) and *ssp245* (**e**) scenarios; **d**, **f** same as (**c**, **e**) but for the ensemble average AMV index. In panels **c**–**f**, dots indicate non-significant trends.

probable (66%) outcome, with a cold phase being slightly less probable than a warm phase (14% and 20%, respectively). Simulations yielding a pronounced mid-21st-century cold phase of the AMV (ACCESS-CM2 r2; CNRM-CM6-1 r2; MRI-ESM2-0 r3) are compatible with recently published AMV scenarios[17], but disagree on amplitude as well as timing and duration of the anomaly.

There is more uncertainty to account for in the exploration of near-future AMV evolution than considered here, for instance, climate projections neglect the effects of natural forcings[37], but a cluster of volcanic eruptions may well trigger a strong temporary global cold phase in the future as it did in the past[35]. Analog uncertainties stem from remote sources of North Atlantic SST variability, such as El Niño-Southern Oscillation[38], that might have significantly contributed to the recent warm anomaly of the AMV and will continue shaping its future evolution. Our stochastic trend approach neglects an explicit representation of the relationships between the AMV and the global SST, as we acknowledge that discerning both signals is difficult due to their co-phase[25] and a clear-cut separation, as done for some AMV definitions[23], implicates tight assumptions about the AMV as a source of global variability. Finally, the signal-to-noise paradox[39] provides an additional framework to interpret the developing incoherences across the AMV scenario evolutions: accordingly, if models underestimate the observed signal-to-noise ratio of the AMV[27], then simulations contain a smaller proportion of predictable variance than the observations, and hence the real-world is more predictable than the models. In this case, the near-future evolution of the AMV will provide clearer information about its damped character than what is discernible by current climate simulations.

Notwithstanding uncertainties, if our interpretation of the AMV is correct, it is only a matter of time—less than a decade even for the most optimistic models and scenario with a current warming of ~0.11 °C/decade—for the predominance of accelerated North Atlantic warming over the AMV warming to become incontrovertible.

Methods

Observational data

SST data for the period 1870–2023 are from the Hadley Centre Sea Ice and Sea-Surface Temperature dataset (HadISST1)[40] available at www.metoffice.gov.uk/hadobs/hadisst/data/download.html and provided on a 1° longitude by 1° latitude global grid. Annual-average data are obtained from the raw monthly time series.

The Kaplan SST AMO index[7] is the unsmoothed long (1856-2022) monthly time series calculated at NOAA PSL1 from the Kaplan SST V2 and available at www.psl.noaa.gov/data/timeseries/AMO/. Annual-average data are obtained from the raw monthly time series.

CMIP6 data

The multi-model ensemble of ocean surface temperature data (variable *tos*) consists of output from 29 coupled climate and Earth system models contributing to the CMIP6 *historical* and *ssp585* experiments for a total of 176 simulations covering the period 1850-2099. The considered models and realizations (in brackets) are ACCESS-CM2 (r{1:5}), ACCESS-ESM1-5 (r{1:40}), AWI-CM-1-1-MR (r1), BCC-CSM2-MR (r1), CAMS-CSM1-0 (r{1,2}), CAS-ESM2-0 (r{1,3}), CESM2-WACCM (r{1:5}), CMCC-ESM2 (r1), CNRM-CM6-1-HR (r1), CNRM-CM6-1 (r{1:6}), CNRM-ESM2-1 (r{1:5}), CanESM5 (r{1:25}), EC-Earth3 (r{1,3,4,6}), FGOALS-g3 (r{1:4}), FIO-ESM-2-0 (r{1:3}), GFDL-CM4 (r1), GFDL-ESM4 (r1), GISS-E2-1-G (r1), INM-CM4-8 (r1), INM-CM5-0 (r1), IPSL-CM6A-LR (r{1:4,6,14,33}), MIROC-ES2L (r{2:10}), MIROC6 (r{1:10}), MPI-ESM1-2-HR (r{1:2}), MPI-ESM1-2-LR (r{1:9,11:30}), MRI-ESM2-0 (r5), NorESM2-LM (r1), NorESM2-MM (r1), and TaiESM1 (r1). Details on the models contributing to the multi-model ensemble are provided in Table 1. The Atlantic meridional overturning circulation is assessed using annual means of data for the Atlantic basin from the *msftmz* or the *msftyz* variable, depending on availability. For the AMV sub-ensemble we also use data from the *ssp245* experiment. Other scenarios are not expected to differ significantly from the scenarios considered here during the first decades of the 21st-century, as trajectories typically diverge only during the second half of the century[29]. The data are retrieved through the Earth System Grid Federation (ESGF) service. Annual-average data are obtained from the raw monthly time series.

AMV and global-mean SST indices

North Atlantic average SST is calculated as the cell area-weighted average of gridded annual-average SST data over the North Atlantic, from the equator to 60°N latitude and between 75°W and 5 °W longitude (AMV domain). Then, three AMV indices are defined based on the North Atlantic average SST. Two AMV indices are defined over the historical period 1870–2023 as the time series of residuals from the least-square fitting to the North Atlantic average SST with time as a predictor and using a second-order (quadratic trend) and first-order (linear trend) polynomial. A third AMV index is

Table 1 | Details of the climate model data contributing to the multi-model ensemble

Acronym	Institution ID	Data reference (*historical*)	Doi (*historical*, scenarios)
ACCESS-CM2	CSIRO-ARCCSS	Dix, Martin et al. (2019). CSIRO-ARCCSS ACCESS-CM2 model output prepared for CMIP6 CMIP. Earth System Grid Federation. https://doi.org/10.22033/ESGF/CMIP6.2281	https://doi.org/10.22033/ESGF/CMIP6.2281 https://doi.org/10.22033/ESGF/CMIP6.2285
ACCESS-ESM1-5	CSIRO	Ziehn, Tilo et al. (2019). CSIRO ACCESS-ESM1.5 model output prepared for CMIP6 CMIP. Earth System Grid Federation. https://doi.org/10.22033/ESGF/CMIP6.2288	https://doi.org/10.22033/ESGF/CMIP6.2288 https://doi.org/10.22033/ESGF/CMIP6.2291
AWI-CM-1-1-MR	AWI	Semmler, Tido et al. (2018). AWI AWI-CM1.1MR model output prepared for CMIP6 CMIP. Earth System Grid Federation. https://doi.org/10.22033/ESGF/CMIP6.359	https://doi.org/10.22033/ESGF/CMIP6.359 https://doi.org/10.22033/ESGF/CMIP6.376
BCC-CSM2-MR	BCC	Xin, Xiaoge et al. (2018). BCC BCC-CSM2MR model output prepared for CMIP6 CMIP. Earth System Grid Federation. https://doi.org/10.22033/ESGF/CMIP6.1725	https://doi.org/10.22033/ESGF/CMIP6.1725 https://doi.org/10.22033/ESGF/CMIP6.1732
CAMS-CSM1-0	CAMS	Rong, Xinyao (2019). CAMS CAMS_CSM1.0 model output prepared for CMIP6 CMIP. Earth System Grid Federation. https://doi.org/10.22033/ESGF/CMIP6.1399	https://doi.org/10.22033/ESGF/CMIP6.1399 https://doi.org/10.22033/ESGF/CMIP6.11004
CanESM5	CCCma	Swart, Neil Cameron et al. (2019). CCCma CanESM5 model output prepared for CMIP6 CMIP. Earth System Grid Federation. https://doi.org/10.22033/ESGF/CMIP6.1303	https://doi.org/10.22033/ESGF/CMIP6.1303 https://doi.org/10.22033/ESGF/CMIP6.1317
CAS-ESM2-0	CAS	Chai, Zhaoyang (2020). CAS CAS-ESM2.0 model output prepared for CMIP6 CMIP. Earth System Grid Federation. https://doi.org/10.22033/ESGF/CMIP6.1944	https://doi.org/10.22033/ESGF/CMIP6.1944 https://doi.org/10.22033/ESGF/CMIP6.1957
CESM2-WACCM	NCAR	Danabasoglu, Gokhan (2019). NCAR CESM2-WACCM model output prepared for CMIP6 CMIP. Earth System Grid Federation. https://doi.org/10.22033/ESGF/CMIP6.10024	https://doi.org/10.22033/ESGF/CMIP6.10024 https://doi.org/10.22033/ESGF/CMIP6.10026
CMCC-ESM2	CMCC	Lovato, Tomas et al. (2021). CMCC CMCC-ESM2 model output prepared for CMIP6 C4MIP. Earth System Grid Federation. https://doi.org/10.22033/ESGF/CMIP6.13164	https://doi.org/10.22033/ESGF/CMIP6.13163 https://doi.org/10.22033/ESGF/CMIP6.13168
CNRM-CM6-1-HR	CNRM-CERFACS	Voldoire, Aurore (2019). CNRM-CERFACS CNRM-CM6-1-HR model output prepared for CMIP6 CMIP. Earth System Grid Federation. https://doi.org/10.22033/ESGF/CMIP6.1385	https://doi.org/10.22033/ESGF/CMIP6.1385 https://doi.org/10.22033/ESGF/CMIP6.1388
CNRM-CM6-1	CNRM-CERFACS	Voldoire, Aurore (2018). CNRM-CERFACS CNRM-CM6-1 model output prepared for CMIP6 CMIP. Earth System Grid Federation. https://doi.org/10.22033/ESGF/CMIP6.1375	https://doi.org/10.22033/ESGF/CMIP6.1375 https://doi.org/10.22033/ESGF/CMIP6.1384
CNRM-ESM2-1	CNRM-CERFACS	Seferian, Roland (2018). CNRM-CERFACS CNRM-ESM2-1 model output prepared for CMIP6 CMIP. Earth System Grid Federation. https://doi.org/10.22033/ESGF/CMIP6.1391	https://doi.org/10.22033/ESGF/CMIP6.1391 https://doi.org/10.22033/ESGF/CMIP6.1395
EC-Earth3	EC_Earth-Consortium	EC-Earth Consortium (EC-Earth) (2019). EC-Earth-Consortium EC-Earth3 model output prepared for CMIP6 CMIP. Earth System Grid Federation. https://doi.org/10.22033/ESGF/CMIP6.181	https://doi.org/10.22033/ESGF/CMIP6.181 https://doi.org/10.22033/ESGF/CMIP6.251
FGOALS-g3	CAS	Li, Lijuan (2019). CAS FGOALS-g3 model output prepared for CMIP6 CMIP. Earth System Grid Federation. https://doi.org/10.22033/ESGF/CMIP6.1783	https://doi.org/10.22033/ESGF/CMIP6.1783 https://doi.org/10.22033/ESGF/CMIP6.2056
FIO-ESM-2-0	FIO-QLNM	Song, Zhenya et al. (2019). FIO-QLNM FIO-ESM2.0 model output prepared for CMIP6 CMIP. Earth System Grid Federation. https://doi.org/10.22033/ESGF/CMIP6.9047	https://doi.org/10.22033/ESGF/CMIP6.9047 https://doi.org/10.22033/ESGF/CMIP6.9051
GFDL-CM4	NOAA-GDFL	Zhao, Ming et al. (2018). NOAA-GFDL GFDL-AM4 model output. Earth System Grid Federation. https://doi.org/10.22033/ESGF/CMIP6.1401	https://doi.org/10.22033/ESGF/CMIP6.1401 https://doi.org/10.22033/ESGF/CMIP6.9242
GFDL-ESM4	NOAA-GFDL	Krasting, John P. et al. (2018). NOAA-GFDL GFDL-ESM4 model output prepared for CMIP6 CMIP. Earth System Grid Federation. https://doi.org/10.22033/ESGF/CMIP6.1407	https://doi.org/10.22033/ESGF/CMIP6.1407 https://doi.org/10.22033/ESGF/CMIP6.1414

Table 1 (continued) | Details of the climate model data contributing to the multi-model ensemble

Acronym	Institution ID	Data reference (*historical*)	Doi (*historical*, scenarios)
GISS-E2-1-G	NASA-GISS	NASA Goddard Institute for Space Studies (NASA/GISS) (2018). NASA-GISS GISS-E2.1G model output prepared for CMIP6 CMIP. Earth System Grid Federation. https://doi.org/10.22033/ESGF/CMIP6.1400	https://doi.org/10.22033/ESGF/CMIP6.1400 https://doi.org/10.22033/ESGF/CMIP6.2074
INM-CM4-8	INM	Volodin, Evgeny et al. (2019). INM INM-CM4-8 model output prepared for CMIP6 CMIP. Earth System Grid Federation. https://doi.org/10.22033/ESGF/CMIP6.1422	https://doi.org/10.22033/ESGF/CMIP6.1422 https://doi.org/10.22033/ESGF/CMIP6.12322
INM-CM5-0	INM	Volodin, Evgeny et al. (2019). INM INM-CM5-0 model output prepared for CMIP6 CMIP. Earth System Grid Federation. https://doi.org/10.22033/ESGF/CMIP6.1423	https://doi.org/10.22033/ESGF/CMIP6.1423 https://doi.org/10.22033/ESGF/CMIP6.12322
IPSL-CM6A-LR	IPSL	Boucher, Olivier et al. (2018). IPSL IPSL-CM6A-LR model output prepared for CMIP6 CMIP. Earth System Grid Federation. https://doi.org/10.22033/ESGF/CMIP6.1534	https://doi.org/10.22033/ESGF/CMIP6.1534 https://doi.org/10.22033/ESGF/CMIP6.1532
MIROC-ES2L	MIROC	Hajima, Tomohiro et al. (2019). MIROC MIROC-ES2L model output prepared for CMIP6 CMIP. Earth System Grid Federation. https://doi.org/10.22033/ESGF/CMIP6.902	https://doi.org/10.22033/ESGF/CMIP6.902 https://doi.org/10.22033/ESGF/CMIP6.936
MIROC6	MIROC	Tatebe, Hiroaki; Watanabe, Masahiro (2018). MIROC MIROC6 model output prepared for CMIP6 CMIP. Earth System Grid Federation. https://doi.org/10.22033/ESGF/CMIP6.881	https://doi.org/10.22033/ESGF/CMIP6.881 https://doi.org/10.22033/ESGF/CMIP6.898
MPI-ESM1-2-HR	MPI-M; DWD	Jungclaus, Johann et al. (2019). MPI-M MPIESM1.2-HR model output prepared for CMIP6 CMIP. Earth System Grid Federation. https://doi.org/10.22033/ESGF/CMIP6.741	https://doi.org/10.22033/ESGF/CMIP6.741 https://doi.org/10.22033/ESGF/CMIP6.4479
MPI-ESM1-2-LR	MPI-M	Wieners, Karl-Hermann et al. (2019). MPI-M MPIESM1.2-LR model output prepared for CMIP6 CMIP. Earth System Grid Federation. https://doi.org/10.22033/ESGF/CMIP6.742	https://doi.org/10.22033/ESGF/CMIP6.742 https://doi.org/10.22033/ESGF/CMIP6.6705 https://doi.org/10.22033/ESGF/CMIP6.6693
MRI-ESM2-0	MRI	Yukimoto, Seiji et al. (2019). MRI MRI-ESM2.0 model output prepared for CMIP6 CMIP. Earth System Grid Federation. https://doi.org/10.22033/ESGF/CMIP6.621	https://doi.org/10.22033/ESGF/CMIP6.621 https://doi.org/10.22033/ESGF/CMIP6.638
NorESM2-LM	NCC	Seland, Øyvind et al. (2019). NCC NorESM2-LM model output prepared for CMIP6 CMIP. Earth System Grid Federation. https://doi.org/10.22033/ESGF/CMIP6.502	https://doi.org/10.22033/ESGF/CMIP6.502 https://doi.org/10.22033/ESGF/CMIP6.604
NorESM2-MM	NCC	Bentsen, Mats et al. (2019). NCC NorESM2-MM model output prepared for CMIP6 CMIP. Earth System Grid Federation. https://doi.org/10.22033/ESGF/CMIP6.506	https://doi.org/10.22033/ESGF/CMIP6.506 https://doi.org/10.22033/ESGF/CMIP6.608
TaiESM1	AS-RCEC	Lee, Wei-Liang; Liang, Hsin-Chien (2019). AS-RCEC TaiESM1.0 model output prepared for CMIP6 CMIP. Earth System Grid Federation. https://doi.org/10.22033/ESGF/CMIP6.9684	https://doi.org/10.22033/ESGF/CMIP6.9684 https://doi.org/10.22033/ESGF/CMIP6.9688

defined over the 1870–2023 period for HadISST data and the 1870-2099 period for the simulated data as the residual of a dynamic linear model (dlm) fit the North Atlantic average SST considering a local stochastic trend (see below).

Global-mean SST is calculated as the cell area-weighted average of gridded annual-average SST data over the world ocean between 60°S and 60°N latitude excluding data from the AMV domain. A fourth AMV index is then defined following[23] as the difference between the North Atlantic and the global-mean SST, with the temporal average removed to obtain anomalies around zero. This index assumes that the SST evolution outside the North Atlantic is independent of the AMV.

Statistical analyses

Statistical significance of differences between data for the two warm AMV periods are estimated using a two-sided rank sum test that is equivalent to the Mann–Whitney *U*-test.

Temporal correlation coefficients and root mean squared errors between simulated and observed AMV indices are calculated for the period 1870–2023. Spatial correlations and spatial root mean squared errors between simulated and observed AMV patterns are calculated from the least-squares regression patterns of the AMV index on the gridded SSTs over the AMV domain, accounting for cell area weights. Ensemble-mean spatial patterns shown in Fig. 2 and Fig. 4 are obtained with a two-step process: first, the single-model ensemble mean is calculated, and then, the multi-model mean is calculated from the single-model ensemble means.

The skills of statistical models with least-square fit to the data to describe the trend in average North Atlantic SST are evaluated based on the following metrics: the coefficient of determination (R^2), the Akaike information criterion (AIC), Schwarz's Bayesian criterion (SBC) and the corrected AIC. Based on the model's sum of squared errors *sse*, number of data n and number of parameters p, AIC is calculated as $n \cdot \log(sse/n) + p$, SBC is

calculated as $n{\cdot}\log(sse/n) + p{\cdot}\log(n)$ and AICc is calculated as $n{\cdot}\log(sse/n) + (n+p)/(1\text{-}(p+2)/n)$. The best model is characterized by the highest value of R^2 and the lowest values of AIC, AICc, and SBC.

We fit the ensemble mean AMV index for the AMV sub-ensemble to the general delayed oscillator with form $y'(t) = a{\cdot}y(t) - b{\cdot}y(t\text{-}\delta) - g{\cdot}y^3(t)$ where t is time, y and y' are the AMV index and its derivative through time, respectively, a is the parameter controlling the positive feedback, b is the parameter controlling the delayed negative feedback with time delay δ, and g is the parameter controlling the damping term. For each δ value between 1 year and 20 years, a 100-member ensemble of predictions for the period 1920–2075 is generated by randomly sampling residuals from their 95% confidence interval determined by a least-square fit to the smoothed (11-year running mean) data. The ensemble combining results from all δ values is used for the final envelope (5–95 percentile range) of the predictions.

Anomalies are calculated over the period 1870–2023.

AMV sub-ensemble

The AMV sub-ensembles of *historical* and *ssp585*/*ssp245* simulations are obtained by selecting simulations that have a good representation of both the spatial pattern and the temporal evolution of the observed AMV (quadratic trend removed from North Atlantic SST). This ensures that the real-world dominant processes governing the AMV (i.e., its spatial pattern) and the phasing between intrinsic and externally forced components of the historical AMV (i.e., its temporal evolution) are well captured by the simulation. For each of the considered future scenarios, the AMV sub-ensemble accordingly consists of 25 selected simulations that have a root mean square error between observed and simulated AMV regression patterns smaller than the threshold of 0.6 and a temporal correlation exceeding 0.4 in the period 1900–2023 (simulations noticeably misrepresenting the 21st-century anomaly are excluded). The simulations contributing to the AMV sub-ensembles are: ACCESS-CM2 r2; ACCESS-ESM1-5 r{10,14:16,33,39}; CMRM-CM6-1 r2; CanESM5 r{3,4,8,13,19,20,21,23,24}; GFDL-CM4 r1; GISS-E2-1-G r1; INM-CM4-8 r1; MIROC6 r{4,5}; MPI-ESM1-2-HR r1; MPI-ESM1-2-LR r28; MRI-ESM2-0 r3. Additional AMV sub-ensembles are explored to account for the dependency of results on the selection criteria for realism and for the dominance of ACCESS-ESM1-5 and CanESM5 in the sub-ensemble; results for these additional AMV sub-ensembles confirm the main analysis.

Dynamic linear model

We use a statistical model developed within the dynamic linear model framework[28,33] to extract the process of interest, that is, the North Atlantic average SST trend, from the noisy raw data. The model is built on a system of three equations (see ref. 28 for further details). Given the discrete measurement M (in this case, the observation, or the model output) at discretized time t (in this case, a certain year in the time series), the state δ of the process is defined as $M(t) = \delta(t) + \varepsilon_M(t)$, where ε_M is Gaussian white noise with zero mean and variance 1 °C^2 that includes observational/numerical errors and higher frequency variations with respect to the SST trend, such as interannual variability. Variance of ε_M is progressively reduced in the scenario period (down to 0.1 °C^2) to accommodate the flattening trend at the end of the 21st-century in *ssp245*. The local stochastic trend β determines the evolution of δ as $\delta(t) = \delta(t-1) + \beta(t-1) + \varepsilon_\delta(t)$ where $(t-1)$ indicates the year before year t, and ε_δ is uncorrelated Gaussian white noise with zero mean and variance 10^{-6} °C^2, which allows δ to rise and fall. Dynamics of β are described as a random walk $\beta(t) = \beta(t-1) + \varepsilon_\beta(t)$, where ε_β is uncorrelated Gaussian white noise with zero mean and variance 10^{-6} °C^2. The imposed low values of ε_δ and ε_β allow for a slowly varying trend with preferred interdecadal time scales. The analysis is performed for each model separately, where M is the raw time series of North Atlantic average SST in the case of a single realization and the ensemble-mean time series if multiple realizations are available, so that δ and β more accurately capture the forced response.

Data availability

The gridded monthly output of CMIP6 climate model simulations that provides the raw data for this study is available via the following ESGF portals: USA, PCMDI/LLNL (California)—https://esgf-node.llnl.gov/search/cmip6/; France, IPSL—https://esgf-node.ipsl.upmc.fr/search/cmip6-ipsl/; Germany, DKRZ—https://esgf-data.dkrz.de/search/cmip6-dkrz/; UK, CEDA—https://esgf-index1.ceda.ac.uk/search/cmip6-ceda/. A derived dataset containing annual-average spatially averaged North Atlantic SST and associated state, stochastic trend, and AMV index for the multi-model ensemble used in this study is available in ref. 41.

Code availability

The dynamic linear model uses the function *dlmsmo* developed by M. J. Laine and is available at https://github.com/mjlaine/dlm.

Received: 12 March 2024; Accepted: 17 October 2024;
Published online: 29 October 2024

References

1. Copernicus, Global Climate Highlights 2023. https://climate.copernicus.eu/global-climate-highlights-2023 (2024).
2. Purich, A. & Doddridge, E. W. Record low Antarctic sea ice coverage indicates a new sea ice state. *Commun. Earth Environ.* **4**, 314 (2023).
3. Cheng, L. et al. New record ocean temperatures and related climate indicators in 2023. *Adv. Atmos. Sci.* https://doi.org/10.1007/s00376-024-3378-5 (2024).
4. Li, K., Zheng, F., Zhu, J. & Zeng, Q.-C. El Niño and the AMO sparked the astonishingly large margin of warming in the global mean surface temperature in 2023. *Adv. Atmos. Sci.* https://doi.org/10.1007/s00376-023-3371-4 (2024).
5. Sellitto, P. et al. The unexpected radiative impact of the Hunga Tonga eruption of 15th January 2022. *Commun. Earth Environ.* **3**, 288 (2022).
6. Deser, C., Knutti, R., Solomon, S. & Phillips, A. S. Communication of the role of natural variability in future North American climate. *Nat. Clim. Change* **2**, 775–779 (2012).
7. Enfield, D. B., Mestas-Nunez, A. M. & Trimble, P. J. The Atlantic multidecadal oscillation and its relationship to rainfall and river flows in the continental U.S. *Geophys. Res. Lett.* **28**, 2077–2080 (2001).
8. Zanchettin, D. et al. (2023) Thermohaline patterns of intrinsic Atlantic Multidecadal Variability in MPI-ESM-LR. *Clim. Dyn.* **61**, 2371–2393 (2023).
9. Zanchettin, D., Bothe, O., Müller, W., Bader, J. & Jungclaus, J. H. Different flavors of the Atlantic Multidecadal Variability. *Clim. Dyn.* **42**, 381–399 (2014).
10. Bellucci, A., Mariotti, A. & Gualdi, S. The role of forcings in the twentieth-century North Atlantic Multidecadal Variability: the 1940–75 North Atlantic cooling case study. *J. Clim.* **30**, 7317–7337 (2017).
11. Bellomo, K., Murphy, L. N., Cane, M. A., Clement, A. C. & Polvani, L. M. Historical forcings as main drivers of the Atlantic Multidecadal Variability in the CESM large ensemble. *Clim. Dyn.* **50**, 3687–3698 (2018).
12. Watanabe, M. & Tatebe, H. Reconciling roles of sulphate aerosol forcing and internal variability in Atlantic multidecadal climate changes. *Clim. Dyn.* **53**, 4651–4665 (2019).
13. Zhang, R. et al. Have aerosols caused the observed Atlantic Multidecadal Variability? *J. Atmos. Sci.* **70**, 1135–1144 (2013).
14. Kim, W. M., Yeager, S. G. & Danabasoglu, G. Key role of internal ocean dynamics in Atlantic Multidecadal Variability during the last half century. *Geophys. Res. Lett.* **45**, 13449–13457 (2018).
15. Otterå, O. H., Bentsen, M., Drange, H. & Suo, L. External forcing as a metronome for Atlantic Multidecadal Variability. *Nat. Geosci.* **3**, 688–694 (2010).
16. Frajka-Williams, E., Beaulieu, C. & Duchez, A. Emerging negative Atlantic Multidecadal Oscillation index in spite of warm subtropics. *Sci. Rep.* **7**, 11224 (2017).

17. Omrani, N.-E. et al. Coupled stratosphere-troposphere-Atlantic multidecadal oscillation and its importance for near-future climate projection. *NPJ Clim. Atmos. Sci.* **5**, 59 (2022).
18. Smith, D. M. et al. North Atlantic climate far more predictable than models imply. *Nature* **583**, 796 (2020).
19. Robson, J., Polo, I., Hodson, D. L. R., Stevens, D. P. & Shaffrey, L. C. Decadal prediction of the North Atlantic subpolar gyre in the HiGEM high-resolution climate model. *Clim. Dyn.* **50**, 921–937 (2017).
20. Yeager, S. The abyssal origins of North Atlantic decadal predictability. *Clim. Dyn.* **55**, 2253–2271 (2020).
21. Eyring, V. et al. Overview of the Coupled Model Intercomparison Project Phase 6 (CMIP6) experimental design and organization. *Geosci. Model Dev.* **9**, 1937–1958 (2016).
22. O'Neill, B. C. et al. The Scenario Model Intercomparison Project (ScenarioMIP) for CMIP6. *Geosci. Model Dev.* **9**, 3461–3482 (2016).
23. Sutton, R. T. et al. Atlantic Multidecadal Variability and the U.K. ACSIS program. *Bull. Am. Meteorol. Soc*. 415–425. https://doi.org/10.1175/BAMS-D-16-0266.1 (2018).
24. Yan, X., Zhang, R. & Knutson, T. R. A multivariate AMV index and associated discrepancies between observed and CMIP5 externally forced AMV. *Geophys. Res. Lett.* **47**, 4421–4431 (2019).
25. Zanchettin, D., Bothe, O., Rubino, A. & Jungclaus, J. H. Multi-model ensemble analysis of Pacific and Atlantic SST variability in unperturbed climate simulations. *Clim. Dyn.* **47**, 1073–1090 (2016).
26. Ruprich-Robert, Y. et al. Assessing the climate impacts of the observed Atlantic Multidecadal Variability using the GFDL CM2.1 and NCAR CESM1 global coupled models. *J. Clim.* **30**, 2785–2810 (2017).
27. Kravtsov, S., Grimm, C. & Gu, S. Global-scale multidecadal variability missing in state-of-the-art climate models. *npj Clim. Atmos. Sci.* **1**, 34 (2018).
28. Laine, M., Latva-Pukkila, N. & Kyrölä, E. Analysing time-varying trends in stratospheric ozone time series using the state space approach. *Atmos. Chem. Phys.* **14**, 9707–9725 (2014).
29. Tebaldi, C. et al. Climate model projections from the Scenario Model Intercomparison Project (ScenarioMIP) of CMIP6. *Earth Syst. Dyn.* **12**, 253–293 (2021).
30. Swingedouw, D. et al. Bidecadal North Atlantic ocean circulation variability controlled by timing of volcanic eruptions. *Nat. Commun.* **6**, 6545 (2015).
31. Hausfather, Z. & Peters, G. P. RCP8.5 is a problematic scenario for near-term emissions. *Proc. Natl Acad. Sci. USA* **117**, 27791–27792 (2020).
32. Pielke, R. Jr. et al. Plausible 2005-2050 emission scenarios project between 2 degC and 3 degC of warming by 2100. *Environ. Res. Lett.* **17**, 024027 (2022).
33. Zanchettin, D., Rubinetti, S. & Rubino, A. Is the Atlantic a source for decadal predictability of sea-level rise in Venice? *Earth Space Sci.* **9**, e2022EA002494 (2022).
34. Michel, S. L. L. et al. Early warning signal for a tipping point suggested by a millennial Atlantic Multidecadal Variability reconstruction. *Nat. Commun.* **13**, 5176 (2022).
35. Mann, M. E., Steinman, B. A. & Miller, S. K. Absence of internal multidecadal and interdecadal oscillations in climate model simulations. *Nat. Commun.* **11**, 49 (2020).
36. Falkena, S. K. J., Quinn, C., Sieber, J. & Dijkstra, H. A. A delay equation model for the Atlantic multidecadal oscillation. *Proc. R. Soc. A*, **477**, https://doi.org/10.1098/rspa.2020.0659 (2021).
37. Zanchettin, D. Volcanic eruptions: a source of irreducible uncertainty for future climates. *Geophys. Res. Lett.* **50**, e2023GL105482 (2023).
38. López-Parages, J., Rodríguez-Fonseca, B., Dommenget, D. & Frauen, C. ENSO influence on the North Atlantic European climate: a non-linear and non-stationary approach. *Clim. Dyn.* **47**, 2071–2084 (2016).
39. Scaife, A. A. & Smith, D. A signal-to-noise paradox in climate science. *npj Clim. Atmos. Sci.* **1**, 28 (2018).
40. Rayner, N. A. et al. Global analyses of sea surface temperature, sea ice, and night marine air temperature since the late nineteenth century. *J. Geophys. Res.* **108**, 4407 (2003).
41. Zanchettin, D. North Atlantic average sea-surface temperature in a CMIP6 multi-model ensemble of historical and ssp585/ssp245 simulations [data set]. *Zenodo*. https://doi.org/10.5281/zenodo.13853454 (2024).

Acknowledgements

We acknowledge the World Climate Research Program, which, through its Working Group on Coupled Modeling, coordinated and promoted CMIP6. We thank the climate modeling groups for producing and making available their model output, the ESGF for archiving the data and providing access, and the multiple funding agencies who support CMIP6 and ESGF. Maps are plotted with the m_map package (Pawlowicz 2000) for MATLAB software, using the GSHHG dataset for coastlines. Map colors based on http://www.ColorBrewer.org, by Cynthia A. Brewer, Penn State.

Author contributions

D.Z.: conceptualization, methodology, formal analysis, investigation, data curation, writing—original draft preparation, revision, finalization; A.R.: discussion, writing—revision.

Competing interests

The authors declare no competing interests.

Additional information

Supplementary information The online version contains supplementary material available at https://doi.org/10.1038/s43247-024-01804-x.

Correspondence and requests for materials should be addressed to Davide Zanchettin.

Peer review information *Communications Earth & Environment* thanks the anonymous reviewers for their contribution to the peer review of this work. Primary handling editor: Heke Langenberg. A peer review file is available.